Published in final edited form as:
Nat Energy. 2020 June ; 5(6): 468–477. doi:10.1038/s41560-020-0624-7.

Photochromic dye-sensitized solar cells with light-driven adjustable optical transmission and power conversion efficiency

Quentin Huaulmé[a], **Valid M. Mwalukuku**[a], **Damien Joly**[a], **Johan Liotier**[a], **Yann Kervella**[a], **Pascale Maldivi**[a], **Stéphanie Narbey**[b], **Frédéric Oswald**[b], **Antonio J. Riquelme**[c], **Juan Antonio Anta**[c], **Renaud Demadrille**[a]

[a]CEA-Univ. Grenoble Alpes-CNRS, IRIG, SyMMES, 38000 Grenoble, France

[b]Solaronix SA, Rue de l'Ouriette 129, 1170 Aubonne, Switzerland

[c]Área de Química Física, Departamento de Sistemas Físicos, Químicos y Naturales, Universidad Pablo de Olavide, Sevilla, E-41013 Spain

Abstract

Semi-transparent photovoltaics only allows for the fabrication of solar cells with an optical transmission that is fixed during their manufacturing resulting in a trade-off between transparency and efficiency. For the integration of semi-transparent devices in building, ideally solar cells should generate electricity while offering the comfort for users to self-adjust their light transmission with the intensity of the daylight. Here we report a photochromic dye-sensitized solar cell (DSSC) based on donor-π-conjugated bridge-acceptor structures where the π-conjugated bridge is substituted for a diphenyl-naphthopyran photochromic unit. DSSCs show change in colour and self-adjustable light transmittance when irradiated with visible light and a power conversion efficiency up to 4.17%. The colouration-decolouration process is reversible and these DSSCs are stable over 50 days. We also report semi-transparent photo-chromo-voltaic mini-modules (23 cm^2) exhibiting a maximum power output of 32.5 mW after colouration.

Introduction

Dye-Sensitized Solar Cells (DSSCs) represent a promising photovoltaic technology,[1] since they demonstrate efficiencies higher than 13% at the laboratory-scale,[2–3–4] and 10% in small modules.[5] Thanks to their remarkable performance under various inclinations and irradiation conditions, they are ideal candidates for use under partly shadowed, dim or artificial light environments.[6] Their manufacturing is simple, environmentally acceptable, compatible with

Competing interests declaration.
R.D, D.J, Y.K are employees of CEA which holds a patent on this technology. Inventors : R. Demadrille, D. Joly, Y. Kervella. Current Assignee Commissariat à l'Energie Atomique et aux Energies Alternatives. Application number: 17305597.1 Date of publication: 28.11.2018. S.N is currently employee of Solaronix Company which sells electrodes and chemical components that are used in this study.

Author Contributions
QH, DJ, JL, YK synthesized and characterized the dyes. PM performed the DFT calculations. VMM, SN, FO fabricated, optimized, and characterized the solar cells and mini-modules. AJR and JAA investigated the solar cells by EIS and performed IPCE measurements. RD designed the materials and the experiments. RD treated the data and wrote the manuscript with contributions from all authors. All authors have given approval to the final version of the manuscript.

Europe PMC Funders Author Manuscripts

industrial requirements and large-scale production, and the raw materials are inexpensive.[7] More importantly, DSSCs have demonstrated long-term stability equivalent to 10 years of outdoor operation, [6–8] and they can be semi-transparent and colourful.[9] These points make them appealing elements for Building Integrated PhotoVoltaics (BIPV).[10]

However, when developing semi-transparent solar cells, a trade-off has to be found between transparency and efficiency. Current state-of-the-art of semi-transparent photovoltaics only allows for the fabrication of solar cells showing an optical transmission that is fixed during the fabrication process.[11–12–13–14–15] For the development of smart photovoltaic windows and their massive integration in buildings, solar cells with variable and self-adaptable optical properties would be very valuable. The Grail would be that solar cells, transparent under low light conditions, could tune without any external manipulation their absorption under more intense illumination to produce energy. Recently, to tackle this challenge, a strategy based on the use of photochromic molecules emerged. A photochromic dye is a compound capable of undergoing, upon irradiation, a reversible transformation between two forms displaying different absorption spectra.[16–17] Usually the uncoloured isomer is observed in the dark and the coloured isomer is generated under light. In principle, such molecules could be well adapted to tune the optical absorption/transmission of devices depending on light intensity. However, the dyes that were employed so far in solar cells did not show a reversible photochromic behaviour once activated or they led to very poor performances. For instance, the photo-isomerization process in bis-thienylethene sensitizers is only activated by irradiation.[18] Therefore, interconversion between the different photo-isomers in devices is only permitted by manipulation of light by alternating irradiation with UV and visible light. Furthermore, the formation of the coloured isomers leads to the lowest PCEs, attributed to a poor charge separation. Such photochromic behaviour is obviously not compatible for use in real conditions and practical applications.

Earlier work has reported the use of photochromic spiropyran and spirooxazine dyes in DSSCs.[19–20] After isomerisation, these molecules theoretically show a photo-chemically and thermally activated bleaching process. However, the tested compounds were poorly colourable, their photo-isomerisation in devices required prolonged UV irradiation to yield the coloured isomer. The anchoring function was not conjugated with the photochromic core of the molecules, leading to a bad sensitization of the electrodes; consequently, a poor PCE of around 0.2% after 30 min under UV irradiation was measured. The devices did not show reversibility of the process because the prolonged UV exposure led to the degradation of the dye and consequently of the device performances. To summarize, none of these studies has succeeded to provide efficient solar cells with self-adjustable optical properties.

Herein, to tackle the challenge of solar cells with variable colour and transparency, we propose a design of photochromic sensitizers based on the integration of diphenyl-naphthopyran photochromic dyes into push-pull structures. Using these molecules, we develop solar cells and mini-modules that show variable colours under irradiation and are capable of self-adjusting simultaneously their optical light transmission and photovoltaic efficiency. We demonstrate photochromic solar cells with a maximum power conversion efficiency (PCE) of up to 4.17% while exhibiting a fully reversible change of colour under irradiation.

Europe PMC Funders Author Manuscripts

Design and synthesis of the photochromic photosensitizers

The most efficient organic sensitizers developed nowadays for DSSC applications possess a Donor-(π-conjugated bridge)-Acceptor (D-π-A) type structure with the A unit also acting as an anchoring group.[21–22–23–24] In this study, we followed this generic strategy by replacing the π-conjugated bridge by a photochromic unit. Only few families of photochromic dyes show both photo-chemically and thermally activated back transformation,[25–26] which is however a major requirement for our application in solar cells. The coloured photo-generated isomers must be thermally unstable to switch back to the initial uncoloured species in the absence of light.

We focused our investigations on the diphenyl-naphthopyran photochromic dyes because they fulfil the latter criterion, possess relatively high fatigue resistance and a good photo-colourability.[27] To use these compounds in a DSSC configuration, it is crucial to control the spatial localisation of the frontier orbitals and their associated energy levels. DFT calculations and modelling were carried out, to help us identify the most favourable orientation of the photochromic unit within the Donor-(photochromic bridge)-Acceptor dye's structure. The complete modelling study and computational methodology details are reported in ESI.

Figure 1 (a) shows the chemical structures of the three molecules that were designed and synthesized in this work. The first dye is based on a 3,3-diphenyl-3*H*-naphtho[2,1-b]pyran core, abbreviated as **NPL** (**L**inear), the second on a 2,2-diphenyl-2*H*-naphtho[1,2-b]pyran core, abbreviated as **NPB** (**B**end) and the third on a 2,2-diphenyl-2*H*-indeno[2,1-*f*]naphtho[1,2-*b*]pyran core abbreviated as **NPI** (**I**ndeno-fused). Within the naphthopyran series, the use of an indeno-naphthopyran core, *i.e.* fusing an indene group to the 5,6 positions (*f*-face), is identified as a good strategy to shift the absorption of the closed form of the dyes over 400 nm making them photochromic under less-energetic UV irradiation.[28–29]

Figure 1 (b) presents the mechanism of the photochromic interconversion for a 3,3-diphenyl-[3H]-naphtho[2,1-b]pyran dye and the equilibrium between the closed (uncoloured) and open (coloured) isomers. The activation of these photochromic compounds requires the absorption of UV-photons, and the back reaction is thermally and photochemically activated.[30] After the photo-isomerisation, two major transoid isomers of the opened form are produced, a TC and a TT isomer.[31] The synthetic routes for the preparation of the photochromic dyes are disclosed in ESI (scheme S1). **NPL**, **NPB** and **NPI** are efficiently prepared in less than 8 steps starting from 6-bromonaphthalen-2-ol (**NPL**) or 1-bromo-4-methoxynaphthalene (**NPB** and **NPI**). The electron-donating unit is introduced by palladium-catalysed cross-coupling reactions (Suzuki-Miyaura or Buchwald-Hartwig conditions), whereas the electron-withdrawing anchoring unit is introduced at the final synthetic step by Knoevenagel condensation with cyano-acetic acid. The critical step in their synthesis is the formation of the naphthopyran ring. This condensation reaction involves a Claisen rearrangement of the alkynyl-aryl ethers resulting from the O-alkylation of the naphthol with aryl-propargylic alcohol, followed by a proton shift and an electrocyclic ring closure. The reaction was performed under weakly acidic conditions[32] to avoid the degradation of the propargylic alcohol through a Meyer-Shuster rearrangement.[33]

Optical and photochromic properties of the dyes

Within the photochromic naphthopyran dyes, upon UV irradiation of the ring-closed form (CF), heterolytic cleavage of the C–O bond of the pyranic heterocycle occurs and a rearrangement of the π-conjugated system gives rise to open form isomers (OF) that possess an extended π-conjugated system, thus exhibiting an absorption band in the visible range. The photo-isomerisation produces several isomers, but all of them are thermally unstable and they can switch back to their initial form.[28] Consequently, upon irradiation an equilibrium between the closed and opened forms is reached, this is the PhotoStationnary State (PSS). The optical parameters of the dyes are reported in Table 1 and the absorption spectra of the three dyes in the dark and under illumination are presented in Figure 2. First, it should be highlighted that the dyes in their uncolored form show an intense absorption in the UV range with relatively high molar absorption coefficents (between $4.18 \cdot 10^4$ and $5.30 \cdot 10^4$ $M^{-1}.cm^{-1}$). **NPL** and **NPB** reveal quite similar absorption properties in their closed state, dominated by an intense absorption peak around 346 nm with a λ_{onset} of 400 nm. Upon irradiation, these dyes exhibit an orange-reddish colour, with a a maximum absorption band at 502 nm and 519 nm respectively. The absorption spectrum of **NPI** in its closed form presents a maximum at 318 nm with several shoulders extending the absorption range up to 450 nm.

This result is particularly interesting since to be photoactivated in solar cells, the uncoloured isomer needs to absorb photons above the absorption cut-off of the glass substrate and the metal oxide film. Under irradiation, in solution, **NPI** shows a spectacular change of color turning from light yellow to green, with two main absorption bands whose maxima are located at 450 nm and 605 nm. To the best of our kwowledge, this molecule is the first example of a photochromic naphthopyran derivative exhibiting a green hue.

When the PSS is reached (in less than 60 seconds at 25°C), the irradiation is turned off and the decolouration curves are registered and modelled using:

$$A(t) = a_1 e^{-k_1 t} + a_2 e^{-k_2 t} + A_\infty \qquad \text{(Equation 1)}$$

where, $A(t)$ is the absorbance of the solution, k_n is the thermal decolouration kinetic constant (in s^{-1}) of the n^{th} kinetic process, a_n the amplitude of the kinetics of this process, and A_∞ the residual absorbance. The normalized decolouration curves (recorded in the dark) for **NPL**, **NPB** and **NPI** are compared in Figure 2 (d). The fastest decolouration process is observed with NPL that shows a rapid constant k_1 of $9.8\ 10^{-2}$ s^{-1} and a slow one k_2 of $1.1\ 10^{-3}$ s^{-1}. After 30 seconds, the solution recovers 80% of its transparency and the total bleaching of the solution occurs in less than 60 minutes. On the contrary, **NPB** presents the slowest discoloration process with a k_1 of $1.4\ 10^{-3}$ s^{-1} and a k_2 of $2.0\ 10^{-4}$ s^{-1}. Even after several hours in the dark the solution is not fully decoloured, indicating that the long-lived isomers (TT) are strongly stabilised.[34–35]

Interestingly, the discolouration of **NPI** can be fitted by a mono-exponential equation and the kinetic constant k_1 is relatively high, equals to $2.1\ 10^{-3}$ s^{-1} at 25°C. This result confirms that the indene substitution with bulky substituents (*para*-phenyl-hexyl) is an efficient way to prevent the formation of long-lived stable isomers thanks to the steric hindrance.

Experimental and theoretical determination of energy levels

To better understand how optoelectronic properties of the dyes change by swapping from the closed to the opened form, the energy levels of the frontiers orbitals were evaluated by cyclic voltammetry (CV) in dichloromethane before and after irradiation (see Figure 3, Tables and Figures in ESI).

The experimental results were compared to the energy levels calculated using DFT with the B3LYP hybrid functional, the modelled electron density distribution in the dyes are reported in Figure 3. First, we notice that the three dyes, both in their closed and opened forms, can inject electrons into CB of TiO_2 located at *circa*-4.1 eV since their LUMO energy levels are included between -3.2 eV and -3.9 eV. Their HOMO energy levels, lying between -5.1 and 5.2 eV, are properly positioned with respect to I^-/I_3^- redox potential (-4.95 eV) thus giving a sufficient driving force for regeneration (0.15 eV).[36]

Photovoltaic properties

The photovoltaic performances of the photochromic dyes were measured in DSSC configuration with a mask under standard irradiation conditions (AM1.5G, 1000 $W.m^{-2}$ simulated solar light, calibrated with a certified silicon solar cell, at 25°C). The solar cells were characterized in the dark and under irradiation after different times of exposure to light. The current-voltage characteristics were recorded at different time intervals to determine the short-circuit current density (J_{sc}), the open-circuit voltage (V_{oc}), the fill factor (FF), and the power conversion efficiency (PCE). We fabricated transparent and opaque solar cells with two types of photo-electrodes based on screen-printed mesoporous anatase TiO2 films. Our first intent to use a commercial electrolyte (Iodolyte), whose composition is made up of 0.5 M 1-butyl-3-methyl-imidazolium iodide (BMII), 0.1 M lithium iodide, 0.05 M iodine and 0.5 M *tert*-butyl-pyridine (*t*BP) in acetonitrile, led to poor performances. However, we observed a drastic change in the colour of the electrode under irradiation accompanied with an increase of J_{sc}. The colouration process was fully reversible, demonstrating for the first time that naphthopyran photochromic dyes can be employed as photosensitizers in solar cells. Based on these preliminary results, we optimized electrolyte composition focusing on the dye with the best absorption, **NPI**. (See ESI). A simple electrolyte with 0.5 M (tBP), 0.1 M lithium iodide, and Iodine was tested. We found an optimum iodine concentration of 0.09 M, leading to a J_{sc} of 3.23 $mA.cm^{-2}$, a V_{oc} of 0.62 V and a FF of 0.75 yielding a PCE of 1.48% at this stage (see ESI).

Second, we optimized the *t*BP concentration, which is often employed to shift the CB of TiO_2 through surface dipole interaction.[37] This methodology was driven by the results from CV experiments reported in the previous section. Indeed, we estimated that the LUMO level of the open isomers of **NPI** is lying at -3.9 eV. This may reduce the driving force for the electron photo-injection. By getting rid of tBP in the electrolyte, it is hence possible to shift back the CB of the oxide, resulting in a better electronic injection.[38–39] To check this hypothesis, a series of solar cells were fabricated using the optimum concentration of iodine that we previously determined and varying the amount of tBP from 0 to 0.5 M. The effect on the photocurrent was spectacular and the J_{sc} values without tBP increased from 2.76 to 10.44 $mA.cm^{-2}$. The PCE of these devices reached 3.69% (see ESI). To get direct

comparison of the performances of **NPL**, **NPB** and **NPI**, we fabricated solar cells using the best conditions that we found for **NPI** dye, *i.e.* with a ratio dye/CDCA of 1/10 for the dyeing bath, and an electrolyte composition of 0.09 M I_2, 0.5 M LiI in acetonitrile. Figure 4 shows the J(V) curves for the DSSCs fabricated with the three dyes before irradiation and after different times of exposure to light, alongside with the pictures of the devices taken before and after irradiation. The detailed photovoltaic parameters of the solar cells are summarized in Table 2. The coloration of **NPL** is extremely faint despite the fact that the dye loading on the mesoporous electrode is the highest. This might be related to: first, the low absorption of **NPL** above 400 nm, which means that the activation of the closed form is not very efficient (due to screen effect of TiO_2 and electrolyte) and second a lower absorption at the PSS because of a strong tendency to revert quickly to the closed form. Consequently, **NPL** yielded the lowest J_{sc} of 4.11 mA.cm^{-2} and the lowest PCE around 1.4%.

On the contrary, the colour changes for **NPB** and **NPI** are more spectacular. Under irradiation, **NPB**-based solar cells become reddish whereas **NPI**-based solar cells switch to dark green. For these dyes, extending the absorption range of the coloured isomers towards the visible region and slowing down the decolouration kinetics compared to **NPL**, result in better photosensitization at the PSS. This led to a significant increase of the J_{sc} reaching 6.94 mA.cm^{-2} and 12.59 mA.cm^{-2} for **NPB** and **NPI** respectively. Interestingly, the best J_{sc} is obtained with the bulkiest dye, *i.e.* the one showing the lowest dye loading on electrodes. The increase in the J_{sc} is in good agreement with the higher absorption properties of the coloured species of this photochromic dye. The best performances are obtained using **NPI** with a mean value of 3.78% (for 21 devices). Our champion photochromic cell passed the 4% efficiency barrier, which is the highest performance ever obtained in solar cells using a photochromic compound.

The photo-induced changes of the optical properties of the semi-transparent solar cells were investigated by UV-Vis spectroscopy. Transmission spectra and average visible transmittance (AVT) of the best cells were measured before and after irradiation (see ESI, Figure S54). The initial AVT of the complete devices before activation are spanning from 55% to 61%. After irradiation, at the PSS, the variation of the AVT is minor for NPL (-2%), more pronounced in the case of NPB (-10%) and rather spectacular for NPI (-32%). Then, the photo-chromo-voltaic properties of NPI solar cells were thoroughly studied (see Figure 5).

Due to the iodine-based electrolyte and the absorption of the closed form of the dye, the solar cells in their initial state appear yellow. After irradiation, they turn green and it is clear that the open isomers of the dye are responsible for this drastic change since the maximum absorption is located at 605 nm. IPCE measurements carried out on opaque cells before and after irradiation unambiguously confirm that **NPI** can generate a photocurrent in both states. Figure 5c shows the variation of the AVT under light exposure. Our experiments unambiguously confirm that the solar cells self-adapt their optical transmission as a function of the irradiation time, as well as a function of the power of irradiation (see ESI, Figure S58). As expected, the PCE increases when the cells become darker even under low-light irradiation. We also demonstrate that the photochromic process in a DSSC is fully reversible, whereby full discolouration takes 16 hours but 80% of the initial transparency at 605 nm is recovered in approximately 2 hours (Figure 5d). In this section, we demonstrate the

Europe PMC Funders Author Manuscripts

concept of photo-chromo-voltaic cells; our DSSCs can adapt simultaneously their absorption and transmission of light and their photovoltaic performances depending on the irradiation conditions.

Origin of the voltage drop upon illumination

We noticed that the V_{oc} of these devices are moderate (between 0.48 and 0.54 V) the highest being obtained with **NPI** bearing alkyl chains.[40] We also observed a drop by 20 to 50 mV of the Voc once the PSS is reached. To unravel the origin of this Voc loss upon irradiation we carried out an Electrochemical Impedance Spectroscopy (EIS) study for **NPI** cells in the dark (under a DC applied potential) and under illumination at open-circuit (using red, λ_{red} = 635 nm, blue, λ_{blue} = 465 nm, and white illumination). The measurements applied a 10 mV perturbation in the 10^6 -0.1 Hz frequency range. For the sake of comparison, a parallel EIS study was performed using DSSC made with the non-photochromic reference dye RK1 with both Iodolyte and NPI-optimized electrolyte. Figure 6 displays Nyquist plots for RK1 and **NPI** solar cells in the dark and under illumination.

The main arc appearing at frequencies around 1-50 Hz is known to correspond to the recombination of electrons in the TiO2 with either acceptor species in the electrolyte or oxidized dyes.[41] As a first approximation, the width of this arc is roughly the recombination resistance. As in any typical DSSC, the recombination resistance is lower upon illumination (the recombination arc shrinks)[42–43] in both RK1 reference solar cells and **NPI** photochromic cells. For measurements done in the dark and under red, blue, and white illumination (in this order), activation of the cell in the first two sets of experiments is avoided. Figure 5(c) shows that the recombination resistance (at the same voltage) decreases in the dark > red > blue > white order.

Impedance data are commonly analyzed by fitting to an equivalent circuit. Transmission line model for DSSCs [37]failed to fit adequately the full spectrum obtained for the **NPI** photochromic devices. However, one can still use the recombination part of this circuit only and fitting the recombination arc to a simple -RC-element and extract recombination resistances (R_{ct}) and chemical capacitances (C_{μ}) These parameters are known to vary with potential according to:

$$R_{ct} \sim exp\left(-\frac{\beta_q V}{k_B T}\right) \quad \text{(Equation 2)}$$

$$C_{\mu} \sim exp\left(\frac{\alpha_q V}{k_B T}\right) \quad \text{(Equation 3)}$$

where V is the DC voltage (either applied or V_{oc}), k_B is the Boltzmann constant and T the absolute temperature.[44–45] The β parameter is the reciprocal of ideality factor and lies in typical DSSC between 0.5 and 0.8. The α parameter is the defining parameter of the exponential TiO_2 distribution of intra-band states (typical values in the 0.15-0.35 interval). Chemical capacitances and recombination resistances are found to fit nicely to Eqs (1) and

(2), respectively. (See ESI Table S52 for a collection of α and β values obtained in the analysis)

The chemical capacitances as a function of the DC voltage were plotted (see ESI, Figure S53). The chemical capacitance, for a given voltage, depends on the position of the TiO_2 conduction band and the position of the electrochemical potential of the redox couple. The largest shift in chemical capacitance is found in the **RK1**-Iodolyte cell when compared with the rest. This is not surprising because its concentration of I_2/I^- is quite different from the homemade electrolyte. There is also a small shift between **RK1** and **NPI** cells, probably because these two dyes have different dipoles. However, no shift is detected between non-activated ("close" configuration) and the activated state ("open" configuration) of the **NPI** cells. This observation is important because it indicates that the V_{oc} drop upon illumination is due to kinetic reasons only and not to a shift of the CB caused by the change of configuration of the dye. This interpretation is also supported by DFT calculations. Indeed, we analysed the sensitizers dipole components relative to the surface plane. We found that larger dipole moments are associated to the open forms of the dyes (See ESI table S9 and Figure S3). This should result in a CB energy level upshift and consequently an increase in Voc.[46–47] But in our case after activation of the dyes, we observe a decrease of Voc.

The most striking observation in the EIS analysis is that the slope of the recombination resistance changes dramatically when the cell is in the "activated" state. A β parameter around 1, obtained under blue and white light, is quite different from what is typically observed in DSSCs. Figure 6 (c, d) shows how as a consequence of the large value of β, the drop of the recombination resistance with respect to the "dark" resistance becomes more and more important the larger is the potential. This indicates that there is an acceleration of the recombination rate upon illumination, which explains the decrease of the V_{oc}. In cell labelled as NPI-2, it is found that red light "activates" slightly the dye, because the recombination resistance changes by a small amount. Interestingly, the change is larger with blue light, where the activation of the dye is expected to be more important. The largest change is found with white light. We remind the reader that the EIS experiments were performed in the dark-red-blue-white order and from the highest to the lowest illumination.

In summary, the EIS results revealed that cells with **NPI** dye have typical behavior when they are in the "dark", non-activated state but their ideality factor (β parameter) changes dramatically upon illumination. In contrast, the chemical capacitance remains unaltered between the "dark" and the "activated" state, meaning that the the V_{oc} drop upon illumination is a kinetic effect that accelerates recombination when the dyes turn into its open isomer. The effect becomes more important when the illumination is higher or when the excitation is closer to the blue. The relatively large values of the β parameter (with respect to "normal" DSSCs) shows that there is an enhancement of the recombination rate that adds to the common effect produced by the increase of electron density in the photoanode. This additional effect can be explained by a larger concentration of "open" dye molecules under illumination, which would facilitate the approximation of the tri-iodide acceptors to the TiO_2 surface.

Stability test and large area semi-transparent mini-modules

We performed a preliminary test to assess the stability of our photochromic devices by analyzing the loss of efficiency as a function of time for opaque devices fabricated with **NPI**. The PCE and electrical parameters were recorded at the PSS. Between measurements, we allowed the devices to bleach fully in the dark at 20°C according to ISOS-D1 standard protocol[48] (Figure 7). First, we observed that the PCE rises a bit after few days, due to a better penetration of the electrolyte in the thick mesoporous layers, leading to activation of the entire electrode.[49] The photochromic behavior of the cells is kept over several months, after each measurement the DSSCs fully discolored in 18 h. Under these storage conditions the T_{80}, corresponding to the time necessary to lose 20% of the initial efficiency, is around 1080 hours (45 days) despite the fact that the devices are based on liquid electrolytes not designed for longterm stability. We identified that the loss of the efficiency is related mostly to the J_{sc} drop, the other photovoltaic parameters of the solar cells being less influenced. After 10 months, **NPI**-solar cells still possess a photochromic behavior and retain 20% of their initial PCE, the decay does not seem linear and can be attributed to the leakage or the evaporation of the electrolyte and the degradation of the dye (see ESI, Figure S59 and S60).

For photovoltaic applications, it is also important to assess the possibility for the fabrication of larger area devices. Therefore, we fabricated semi-transparent mini-modules (23 cm^2) using **NPI** as photosensitizer. Five rectangular shape single cells were inter-connected in series using a W-type design with an overall active area of 14 cm^2 representing 60% of the total area. For the fabrication of the mini-module, the optimized homemade liquid electrolyte was used. In order to achieve a good transparency in the visible the thickness of the titania electrode was kept at 8 μm without scattering layer. Figure 8 shows the yellowish mini-module progressively turns to an aesthetic green colour in less than 2 minutes when exposed to the Sun. (see ESI)

At PSS, this device exhibits a maximum a V_{oc} of 2.43 V, an I_{sc} of 23.62 mA and a FF of 56.7, leading to a maximum power output of 32.5 mW. This preliminary result demonstrates that photochromic dyes can be employed for the fabrication of large area devices with quite decent performances, showing variable colours and transparency, paving the way for the development of a new class of multifunctional semi-transparent solar cells and modules.

Conclusion

We have designed, synthesised and characterized a class of push-pull photochromic dyes for application in photovoltaic devices based on diphenyl-naphthopyran photochromic compounds. Under irradiation with visible light, photochromic DSSCs vary their colour, self-adapt their light transmission from 59% (under dark) to 27% (under light), and simultaneously deliver a photocurrent that reaches its maximum when the solar cells are fully coloured at the photo-stationary state, thus demonstrating a PCE of up to 4.17%. We demonstrate that the photochromic dyes, in their different forms, can generate a photocurrent, and that the J_{sc} of the solar cells increases dramatically with the photo-colouration of the electrodes. Thanks to electrochemical impedance spectroscopy, we could identify a mechanism responsible for a decrease of V_{oc} at the photo-stationary state. Finally, we report preliminary results demonstrating that these photochromic solar cells

Europe PMC Funders Author Manuscripts

can be stable over 50 days (using ISOS-D1 ageing test) and we show that photochromic semi-transparent mini-modules with an active surface of 14 cm^2 can be fabricated leading to a 32.5 mW power output. This work paves the way to the development of a new class of semi-transparent solar cells capable to change colour and to show self-adjustable transmission of light.

Methods

Supplementary Material

Refer to Web version on PubMed Central for supplementary material.

Acknowledgements

RD acknowledges ANR for funding through ODYCE project. (Grant agreement No ANR-14-OHRI-0003-01). JL acknowledges CEA for funding through a CFR PhD Grant. PM thanks GENCI (CINES and IDRIS) for HPC resources (Grant 2019-A0060807648). JAA and AR thank Ministerio de Economía y Competitividad of Spain and Agencia Estatal de Investigación (AEI) and EU (FEDER) under grant MAT2016-79866-R and Red de Excelencia “Emerging photovoltaic Technologies” for financial support. AR thanks the Spanish Ministry of Education, Culture and Sports via a PhD grant (FPU2017-03684).

RD acknowledges European Research Council (ERC) for funding. This project has received funding from the under the European Union’s Horizon 2020 research and innovation program (grant agreement No 832606) - Project PISCO.

Data availability

The data that support the plots within this paper and other findings of this study are available in ESI or from the corresponding author on reasonable request.

References

1. Hagfeldt A, Boschloo G, Sun L, Kloo L, Pettersson H. Dye-sensitized solar cells. Chem Rev. 2010; 110: 6595–6663. [PubMed: 20831177]
2. Mathew S, Yella A, Gao P, Humphry-Baker R, Curchod BFE, Ashari-Astani N, Tavernelli I, Rothlisberger U, Nazeeruddin MK, Grätzel M. Dye-sensitized solar cells with 13% efficiency achieved through the molecular engineering of porphyrin sensitizers. Nat Chem. 2014; 6: 242–247. [PubMed: 24557140]
3. Kakiage K, Aoyama Y, Yano T, Oya K, Fujisawa J-I, Hanaya M. Highly-efficient dye-sensitized solar cells with collaborative sensitization by silyl-anchor and carboxy-anchor dyes. Chem Commun. 2015; 51: 15894–15897.
4. Yao Z, Wu H, Li Y, Wang J, Zhang J, Zhang M, Guo Y, Wang P. Dithienopicenocarbazole as the kernel module of low-energy-gap organic dyes for efficient conversion of sunlight to electricity. Energy Environ Sci. 2015; 8: 3192–3197.
5. Green MA, Emery K, Hishikawa Y, Warta W, Dunlop ED. Solar cell efficiency tables (version 47). Prog Photovolt: Res Appl. 2016; 24: 3–11.
6. Cao Y, Liu Y, Zakeeruddin SM, Hagfeldt A, Grätzel M. Direct Contact of Selective Charge Extraction Layers Enables High-Efficiency Molecular Photovoltaics. Joule. 2018; 2: 1108–1117.
7. Fakharuddin A, Jose R, Brown TM, Fabregat-Santiago F, Bisquert J. A perspective on the production of dye-sensitized solar modules. Energy Environ Sci. 2014; 7: 3952–3981.
8. Sauvage F. A review on current status of stability and knowledge on liquid electrolyte-based dye-sensitized solar cells. Advances in Chemistry. 2014. 939525

9. Joly D, Pelleja L, Narbey S, Oswald F, Meyer T, Kervella Y, Maldivi P, Clifford JN, Palomares E, Demadrille R. Metal-free organic sensitizers with narrow absorption in the visible for solar cells exceeding 10% efficiency. Energy Environ Sci. 2015; 8: 2010–2018.
10. Yoon S, Tak S, Kim J, Jun Y, Kang K, Park J. Application of transparent dye-sensitized solar cells to building integrated photovoltaic systems. Building and Environment. 2011; 46: 1899–1904.
11. Li Y, Xu G, Cui C, Li Y. Flexible and semi-transparent organic solar cells. Adv Energy Mater. 2018; 8 1701791
12. Eperon GE, Burlakov VM, Goriely A, Snaith HJ. Neutral Color Semitransparent Microstructured Perovskite Solar Cells. ACS Nano. 2014; 8: 591–598. [PubMed: 24467381]
13. Della Gaspera E, Peng Y, Hou Q, Spiccia L, Bach U, Jasieniak JJ, Cheng Y-B. Ultra-thin high efficiency semi-transparent perovskite solar cells. Nano Energy. 2015; 13: 249–257.
14. Sun J, Jasieniak JJ. Semi-transparent solar cells. J Phys D: Appl Phys. 2017; 50 093001
15. Brus VV, Lee J, Luginbuhl BR, Ko S-J, Bazan GC, Nguyen T-Q. Solution-Processed Semitransparent Organic Photovoltaics: From Molecular Design to Device Performance. Adv Mater. 2019; 31 1900904
16. Guglielmetti, R. Photochromism: Molecules and Systems. Durr, H, Bouas-Laurent, H, editors. Elsevier; Amsterdam: 2003. 314–466.
17. Fihey A, Perrier A, Browne WR, Jacquemin D. Multiphotochromic molecular systems. Chem Soc Rev. 2015; 44: 3719–3759. [PubMed: 25921433]
18. Wu W, Wang J, Zheng Z, Hu Y, Jin J, Zhang Q, Hua J. A strategy to design novel structure photochromic sensitizers for dye-sensitized solar cells. Sci Rep. 2015; 5 8592 [PubMed: 25716204]
19. Ma S, Ting H, Ma Y, Zheng L, Zhang M, Xiao L, Chen Z. Smart photovoltaics based on dye-sensitized solar cells using photochromic spiropyran derivatives as photosensitizers. AIP Advances. 2015; 5 057154
20. Johnson N-M, Smolin YY, Shindler C, Hagaman D, Soroush M, Lau KKS, Ji H-F. Photochromic dye-sensitized solar cells. AIMS Materials Science. 2015; 2: 503–509.
21. Tian, H, Boschloo, G, Hagfeldt, A. Green Chemistry and Sustainable Technology. Springer; Singapore: 2018.
22. Ooyama Y, Harima Y. Photophysical and electrochemical properties, and molecular structures of organic dyes for Dye-Sensitized Solar Cells. ChemPhysChem. 2012; 13: 4032–4080. [PubMed: 22807392]
23. Mishra A, Fischer MKR, Bäuerle P. Metal-free organic dyes for dye-sensitized solar cells: from structure: property relationships to design rules. Angew Chem Int Ed. 2009; 48: 2474–2499.
24. Wang P, Yang L, Wu H, Cao Y, Zhang J, Xu N, Chen S, Decoppet J-D, Zakeeruddin SM, Grätzel M. Stable and Efficient Organic Dye-Sensitized Solar Cell Based on Ionic Liquid Electrolyte. Joule. 2018; 2: 2145–2153.
25. Minkin VI. Photo-, Thermo-, Solvato-, and Electrochromic Spiroheterocyclic Compounds. Chem Rev. 2004; 104: 2751–2776. [PubMed: 15137806]
26. Tamasulo M, Sortino S, White AJP, Raymo FM. Fast and Stable Photochromic Oxazines. J Org Chem. 2005; 70: 8180–8189. [PubMed: 16277345]
27. Chu, NYC. Photochromism: Molecules and Systems. Durr, H, Bouas-Laurent, H, editors. Elsevier; 2003.
28. Coelho PJ, Salvador MA, Oliveira MM, Carvalho LM. Syn Lett. 2006; 6: 1015–1018.
29. Van Gemert, B. Photochromic indeno-fused naphthopyrans. US5645767. 1997.
30. Van Gemert, B, Crano, JC, Guglielmetti, R. Organic Photochromic and Thermochromic Compounds. Vol. 1. Kluwer Academic/Plenum Publishers; New York: 1999. 111–140. Chapter 3
31. Delbaere S, Vermeersch G. NMR characterization of allenyl-naphthol in the photochromic process of 3,3-diphenyl-[3H]-naphtho[2-1,b]pyran. J Photochem Photobiol A: Chem. 2003; 159: 227–232.
32. Frigoli M, Moustrou C, Samat A, Guglielmetti R. Synthesis of New Thiophene-Substituted 3,3-Diphenyl-3H-naphtho[2,1-b]pyrans by Cross-Coupling Reactions, Precursors of Photomodulated Materials. Eur J Org Chem. 2003; 15: 2799–2812.

33. Moustrou C, Rebiere N, Samat A, Guglielmetti R, Yassar AE, Dubest R, Aubard J. Synthesis of Thiophene-Substituted 3H-Naphtho[2,1-b]pyrans, Precursors of Photomodulated Materials. Helv Chim Acta. 1998; 81: 1293–1302.
34. Delbaere S, Luccioni-Houzé B, Bochu C, Teral Y, Campredon M, Vermeersch G. Kinetic and structural studies of the photochromic process of 3H-naphthopyrans by UV and NMR spectroscopy. J Chem Soc, Perkin Trans. 1998; 2: 1153–1158.
35. Demadrille R, Rabourdin A, Campredon M, Giusti G. Spectroscopic characterisation and photodegradation studies of photochromic spiro[fluorene-9,3'-[3'H]-naphtho[2,1-b]pyrans]. J Photochem Photobiol A: Chem. 2004; 168: 143–152.
36. Hamann TW, Jensen RA, Martinson ABF, Van Ryswyk H, Hupp JT. Advancing beyond current generation dye-sensitized solar cells. Energy Environ Sci. 2008; 1: 66–78.
37. Ruhle S, Greenshtein M, Chen S-G, Merson A, Pizem H, Sukenik CS, Cahen D, Zaban A. Molecular Adjustment of the Electronic Properties of Nanoporous Electrodes in Dye-Sensitized Solar Cells. J Phys Chem B. 2005; 109: 18907–18913. [PubMed: 16853434]
38. Huaulmé Q, Aumaitre C, Kontkanen OV, Beljonne D, Sutter A, Ulrich G, Demadrille R, Leclerc N. Functional panchromatic BODIPY dyes with near-infrared absorption: design, synthesis, characterization and use in dye-sensitized solar cells. Beilstein J Org Chem. 2019; 15: 1758–1768. [PubMed: 31435447]
39. Huang SY, Schlichthörl G, Nozik AJ, Grätzel M, Frank AJ. Charge recombination in dye sensitized nanocrystalline T1O2 solar cells. J Phys Chem B. 1997; 101: 2576.
40. Lee YH, Chitumalla KR, Jang BY, Jang J, Thogiti S, Kim J-H. Alkyl chain length dependence of the charge-transfer, recombination and electron diffusion length on the photovoltaic performance in double donor-acceptor-based organic dyes for dye sensitized solar cells. Dyes and Pigments. 2016; 133: 161–172.
41. Fabregat-Santiago F, Garcia-Belmonte G, Mora-Seró I, Bisquert J. Characterization of nano structured hybrid and organic solar cells by impedance spectroscopy. J Phys Chem Chem Phys. 2011; 13: 9083–9118.
42. Wang Q, Ito S, Gratzel M, Fabregat-Santiago F, Mora-Seró I, Bisquert J, Bessho T, Imai H. Characteristics of High Efficiency Dye-Sensitized Solar Cells. J Phys Chem B. 2006; 110: 25210–25221. [PubMed: 17165965]
43. Wang Q, Moser J-E, Grätzel M. Electrochemical Impedance Spectroscopic Analysis of Dye-Sensitized Solar Cells. J Phys Chem B. 2005; 109: 14945–14953. [PubMed: 16852893]
44. Idígoras J, Pellejà L, Palomares E, Anta J-A. The Redox Pair Chemical Environment Influence on the Recombination Loss in Dye-Sensitized Solar Cells. J Phys Chem C. 2014; 118: 3878–3889.
45. Raga SR, Barea EM, Fabregat-Santiago F. Analysis of the Origin of Open Circuit Voltage in Dye Solar Cells. J Phys Chem Lett. 2012; 312: 1629–1634.
46. Chen P, Yum J-H, De Angelis P, Mosconi E, Fantacci S, Moon S-J, Baker HR, Ko J, Nazeeruddin Md K, Grätzel M. High open-circuit voltage solid-state dye-sensitized solar cells with organic dye. Nano Lett. 2009; 9: 2487–2492. [PubMed: 19438193]
47. Liu B, Li X, Liu M, Ning Z, Zhang Q, Li C, Müllen K, Zhu W. Photovoltaic performance of solid-state DSSCs sensitized with organic isophorone dyes: Effect of dye-loaded amount and dipole moment. Dyes and pigments. 2012; 94: 23–27.
48. Khenkin MV, Katz EA, Abate A, et al. Consensus statement for stability assessment and reporting for perovskite photovoltaics based on ISOS procedures. Nat Energy. 2020; 5: 35–49.
49. Zhang Z, Ito S, Moser J-E, Zakeeruddin SM, Grätzel M. Influence of Iodide Concentration on the Efficiency and Stability of Dye-Sensitized Solar Cell Containing Non-Volatile Electrolyte. ChemPhysChem. 2009; 10: 1834–1838. [PubMed: 19472254]

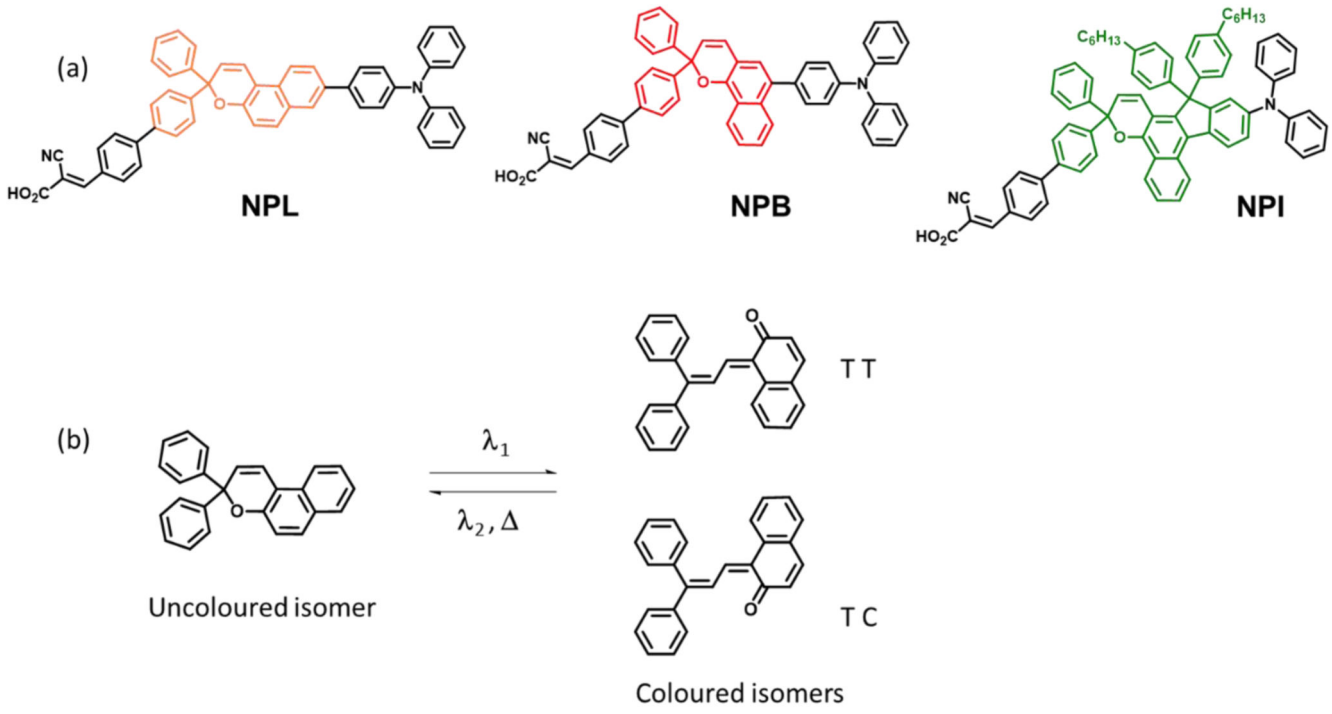

Figure 1.

(a) Chemical structure of the dyes (NPL, NPB, and NPI) synthesized in this work. (b) Example of photochromic interconversion for 3,3-diphenyl-[3H]-naphtho[2,1-b]pyran dye.

Europe PMC Funders Author Manuscripts

Europe PMC Funders Author Manuscripts

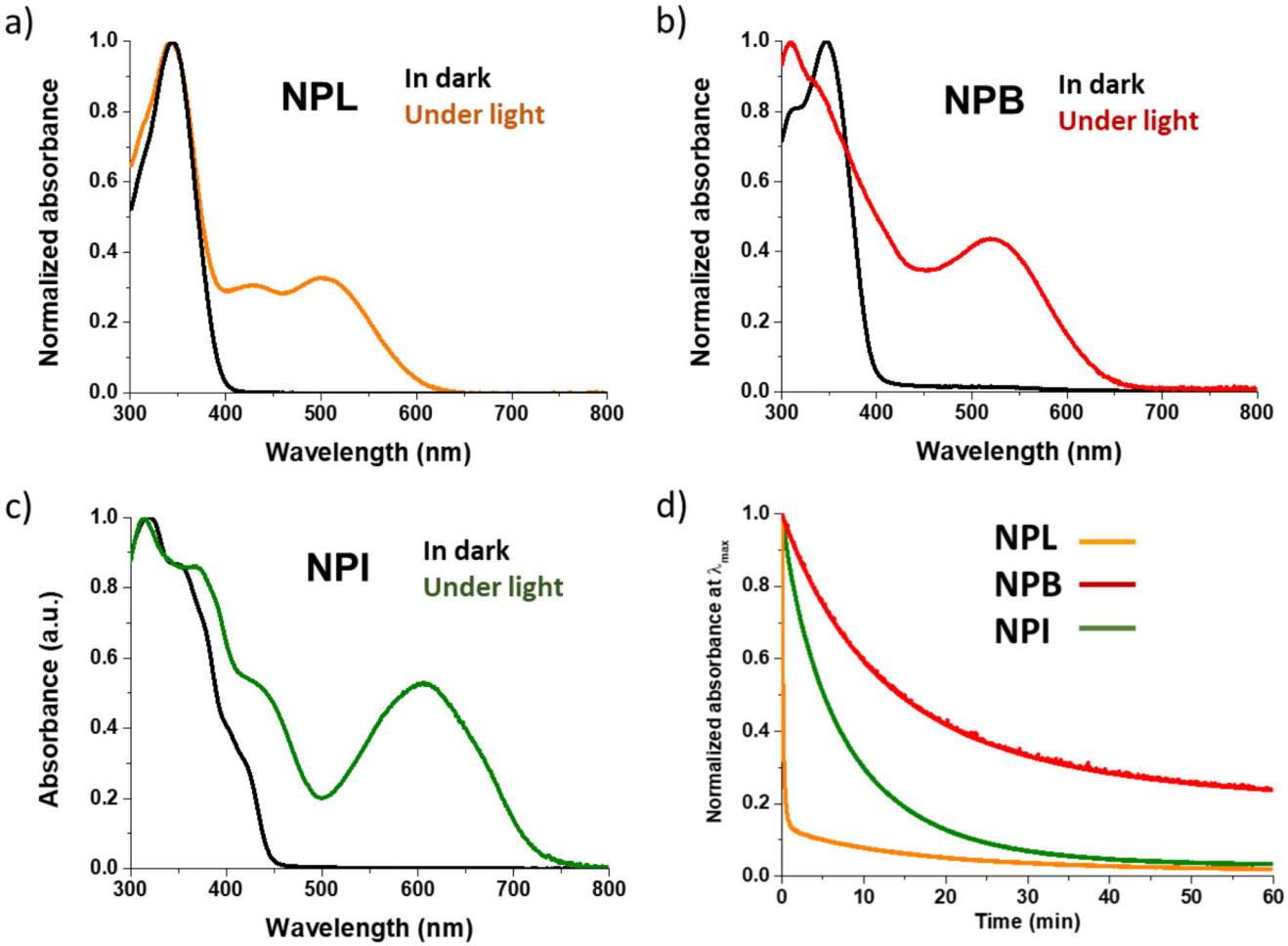

Figure 2.

Normalized absorption spectra of (a) **NPL**, (b) **NPB**, (c) **NPI**, in solution (10^{-5} M in non-degassed toluene) recorded in the dark (black lines) and under irradiation (coloured lines), irradiation conditions (continuous irradiation with a 200W Xenon lamp, equipped with band-pass filter 350-425 nm). (d) Decolouration curves of the dyes recorded in solution in the dark (25°C, 2.10^{-5} M in toluene) after photo-stationary state reached under irradiation with a polychromatic light infrared filtered (200W). The optical density variation was monitored at the λ_{max} of the coloured isomers for each dye.

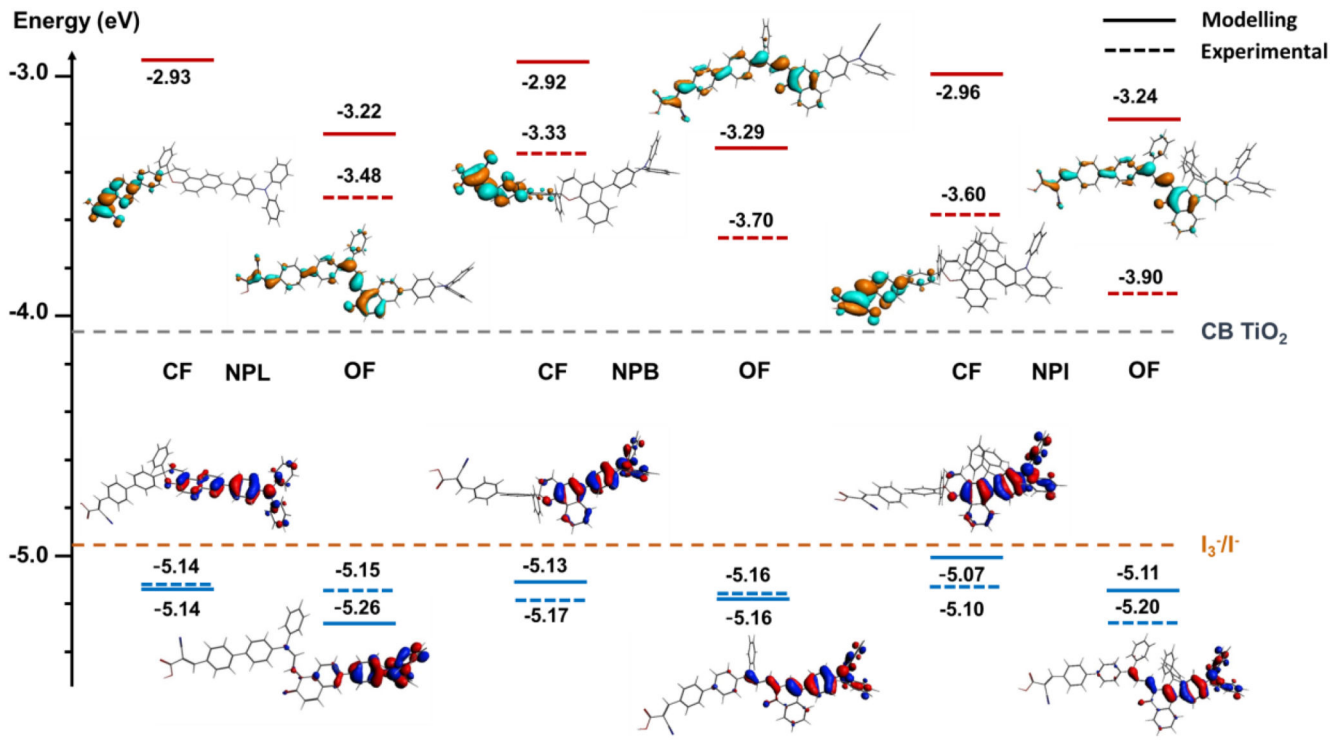

Figure 3.

Experimental and DFT calculated energy levels of the frontier orbitals of the dyes and their spatial localizations (CF, closed form, OF open form trans-isomer). LUMO energy levels are shown in red, HOMO energy levels are shown in blue. The position of the conduction band edge (CB) of the TIO_2 and Nernst potential of the triiodide/iodide redox couple is indicated with a horizontal dashed line with grey and orange colours respectively.

Europe PMC Funders Author Manuscripts

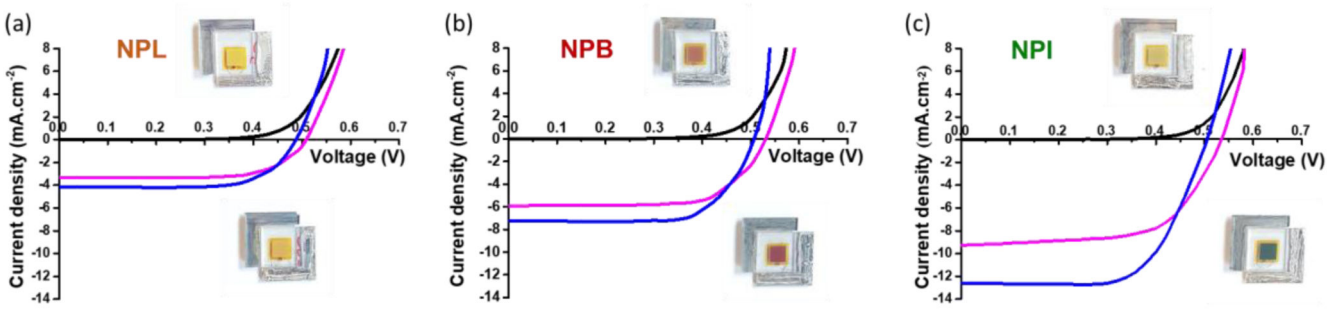

Figure 4.

Current-voltage characteristics of representative opaque photochromic solar cells registered in the dark (black line), after 15 seconds under irradiation (magenta line) and after few minutes of irradiation at the photo-stationary state (blue line) for (a) **NPL**, (b) **NPB** and (c) **NPI**. Insets show of the DSSCs before irradiation (top) and after full coloration under irradiation (bottom).

Europe PMC Funders Author Manuscripts

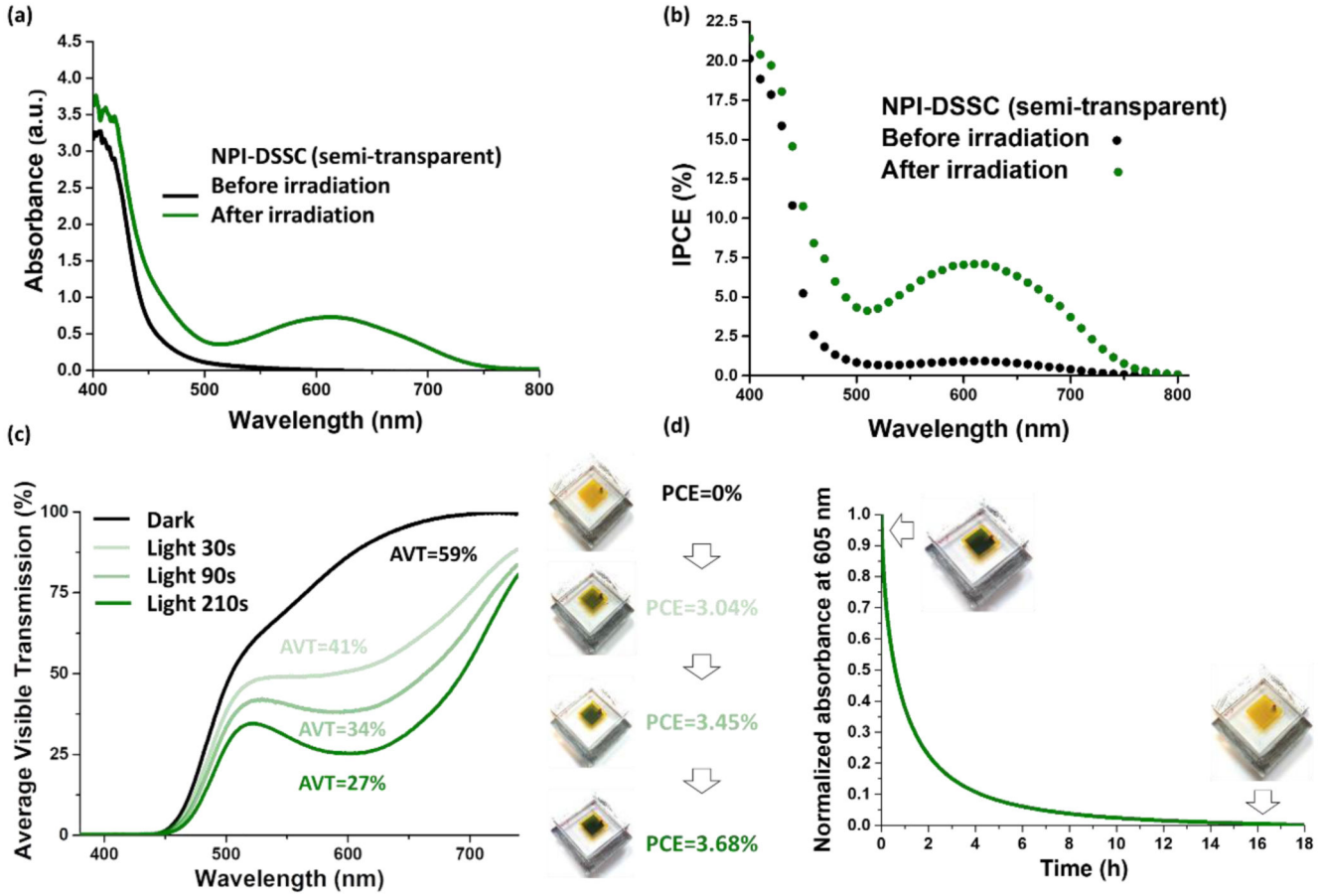

Figure 5.

(a) UV-Vis spectrum of a complete semi-transparent **NPI** based solar cell (13 μm-thick TiO_2) before (black line, yellow solar cell) and after irradiation (green lines, green solar cells), IPCE spectrum of an **NPI**-based transparent solar cell before irradiation (black dots) and at the PSS after activation under irradiation (green dots). (c) Evolution of the Average Visible Transmission (AVT, measured between 380 and 740 nm) and PCE of a semitransparent NPI-based solar cell as a function of light exposure time (standard irradiation conditions). (d) Bleaching curve registered at λmax of a complete semi-transparent **NPI** based solar cell and picture of the cell before and after decolouration.

Europe PMC Funders Author Manuscripts

Europe PMC Funders Author Manuscripts

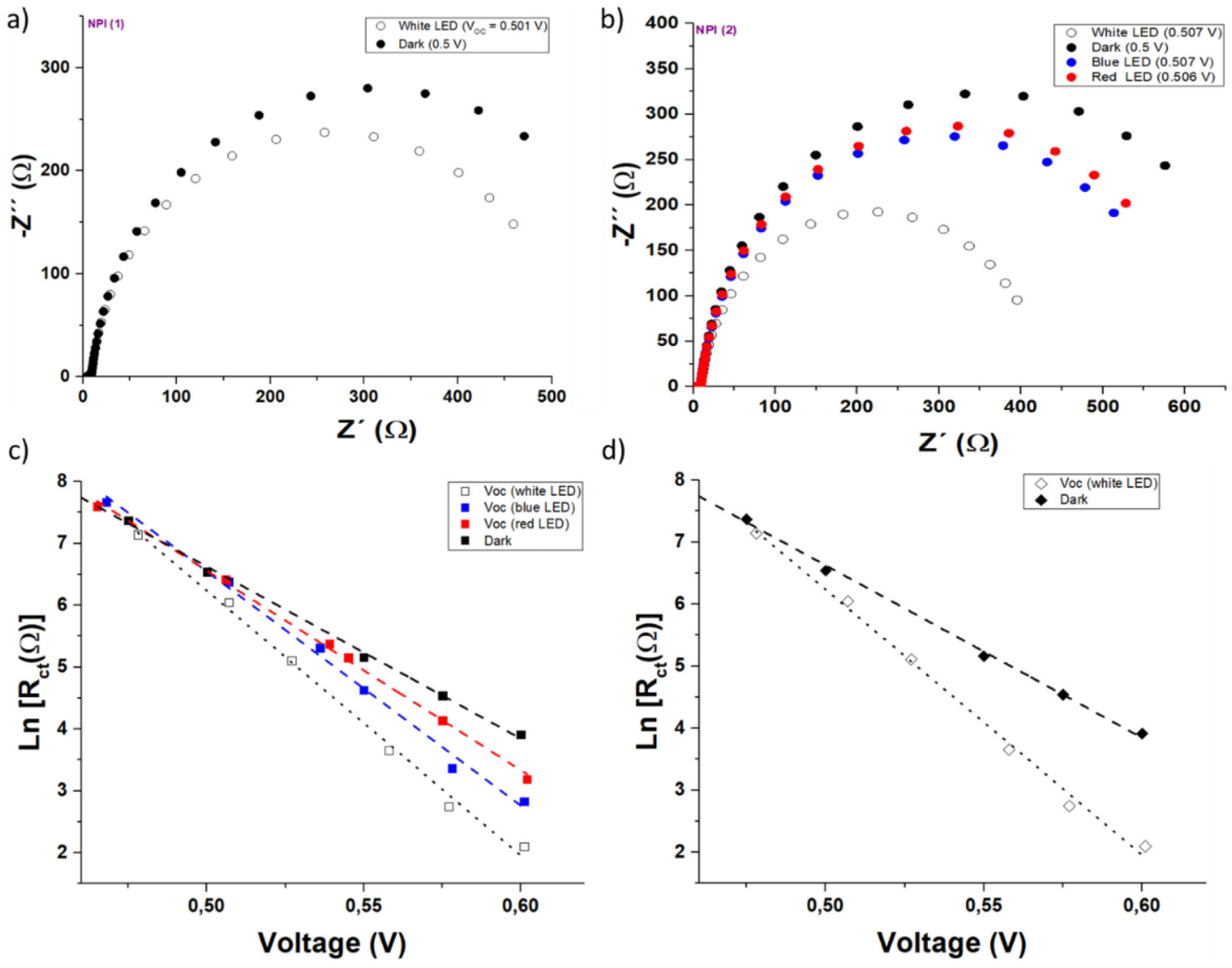

Figure 6.

(a) and (b) Nyquist plots for NPI cells with optimized electrolytes (results for two specimens NPI-1 and NPI-2 are shown). (c) and (d) Recombination resistance as a function of DC voltage (dark) or V_{oc} (light).The latter was fixed by tuning the light illumination intensity. Dashed lines are fits to Eq. (2)

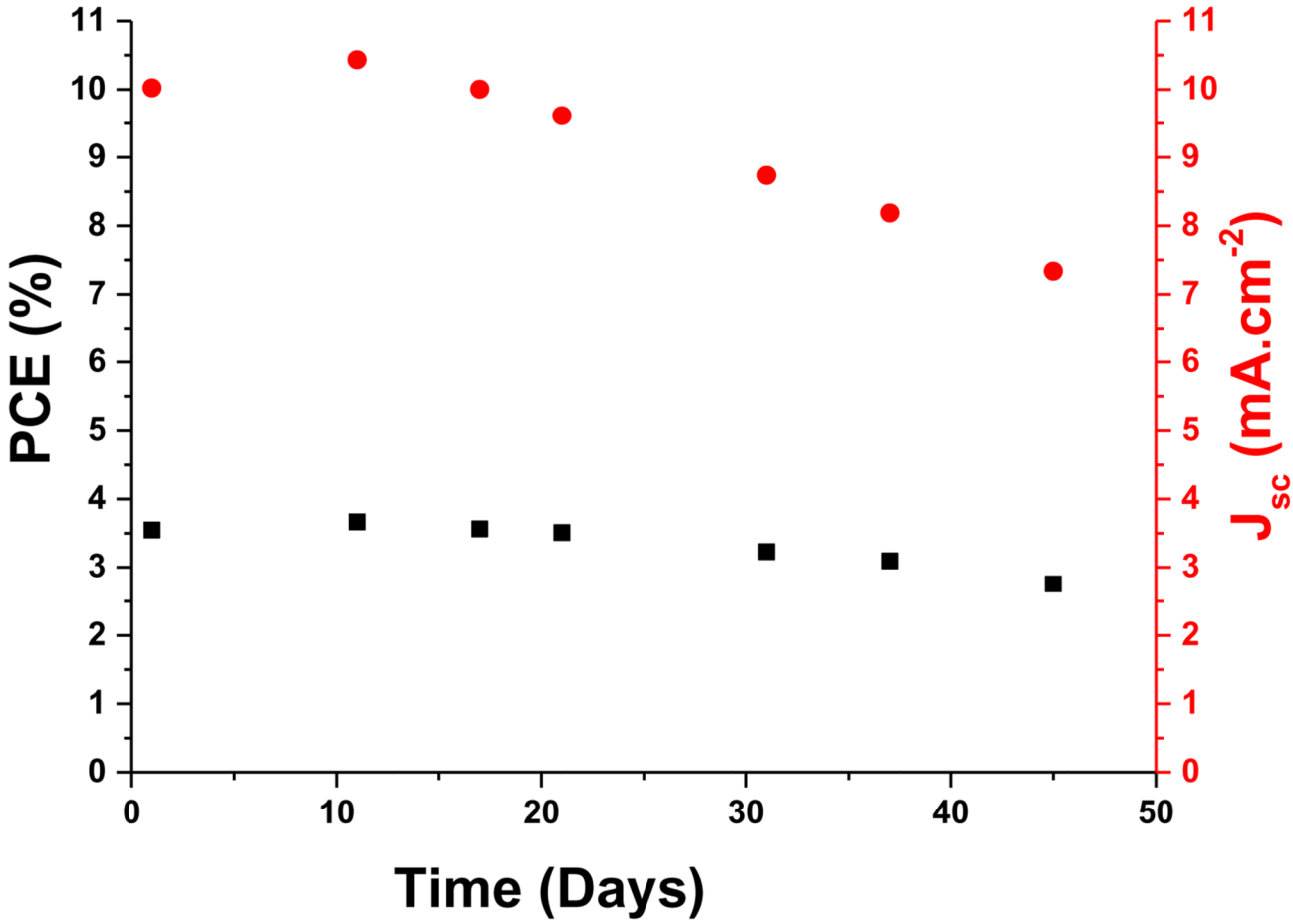

Figure 7. Evolution of the PCE and J_{SC} of NPI-based opaque solar cells, recorded at the PSS over storage time in the dark at 20°C without encapsulation, according to ISOS-D1 standard protocol.

Europe PMC Funders Author Manuscripts

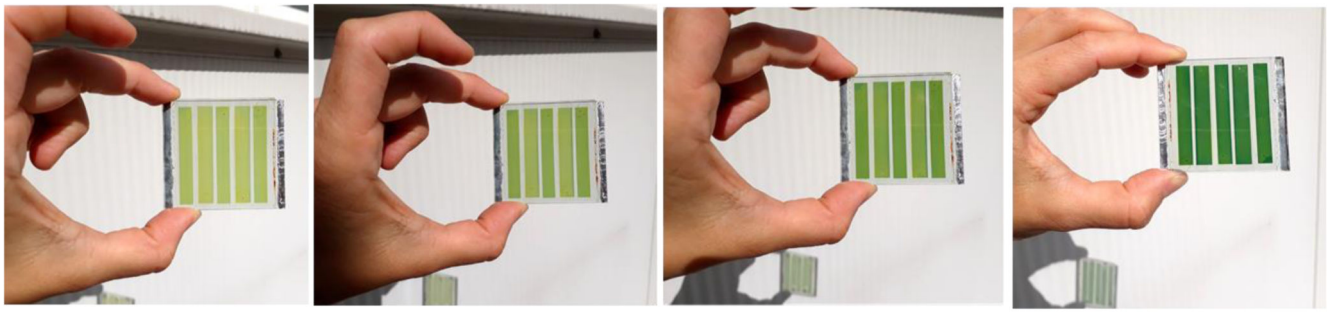

Figure 8. Evolution of the colour of NPI-based solar semi-transparent mini-module when exposed to natural light at 20°C.

Europe PMC Funders Author Manuscripts

Europe PMC Funders Author Manuscripts

Table 1

Optical parameters measured in toluene (10^{-5} M solutions) in the dark (CF) and under continuous irradiation at 25°C, (OF) conditions with a Xenon lamp (200 W).

Dyes	λ_{max} CF	λ_{onset} CF	λ_{max} OF	ε CF	λ_{onset} OF	ΔE_{opt} OF	k_1 at 25°C	k_2 at 25°C
	(nm)	(nm)	(nm)	($M^{-1}.cm^{-1}$)	(nm)	(eV)	(s^{-1})	(s^{-1})
NPL	345	400	519	$5.3\ 10^4$	643	1.93	$9.8\ 10^{-2}$	$1.1\ 10^{-3}$
NPB	347	400	547	$4.5\ 10^4$	636	1.95	$1.4\ 10^{-3}$	$2.0\ 10^{-4}$
NPI	318	450	605	$4.1\ 10^4$	728	1.70	$2.1\ 10^{-3}$	-

Europe PMC Funders Author Manuscripts

Table 2

Dye-loading and photovoltaic parameters of the transparent (13μm-thick TiO_2) and opaque (13μm-thick TiO_2 + 4μm-thick for the scattering layer) DSSCs fabricated with the optimized conditions. In parenthesis: the mean values and deviation obtained from at least 3 devices and 21 devices in the case of NPI opaque cells.

Dyes	Electrode	Jsc ($mA.cm^{-2}$)	Voc (V)	FF	PCE (%)	Dye Loading ($moles.cm^{-2}$)
NPL	Transparent	3.27 (3.07 ± 0.26)	0.513 (0.508 ± 0.004)	0.706 (0.702 ± 0.003)	1.16 (1.09 ± 0.09)	5.56×10^{-7}
	Opaque	4.11 (3.90 ± 0.16)	0.487 (0.493 ± 0.013)	0.732 (0.732 ± 0.008)	1.43 (1.40 ± 0.02)	5.93×10^{-7}
NPB	Transparent	5.62 (5.50 ± 0.13)	0.515 (0.514 ± 0.005)	0.742 (0.739 ± 0.002)	2.15 (2.09 ± 0.04)	4.04×10^{-7}
	Opaque	6.94 (6.62 ± 0.22)	0.513 (0.508 ± 0.003)	0.757 (0.752 ± 0.007)	2.63 (2.53 ± 0.05)	3.95×10^{-7}
NPI	Transparent	10.74 (9.85 ± 1,10)	0.521 (0.515 ± 0.016)	0.658 (0.676 ± 0.029)	3.68 (3.41 ± 0.20)	2.03×10^{-7}
	Opaque	12.59 (10.60 ± 0.95)	0.505 (0.519 ± 0.016)	0.656 (0.692 ± 0.029)	4.17 (3.78 ± 0.18)	2.60×10^{-7}